Structural Characterization of 1:1 van der Waals Complexes of 9-Cyanoanthracene with Aprotic Solvents by Rotational Coherence Spectroscopy

Kazuhiro Egashira, Yasuhiro Ohshima,* and Okitsugu Kajimoto†

Department of Chemistry, Graduate School of Science, Kyoto University, Kitashirakawa-Oiwakecho, Sakyo-ku, Kyoto 606-8502, Japan

Received: January 23, 2001; In Final Form: February 28, 2001

Structures of 9-cyanoanthracene (CNA) clusters microsolvated with a single molecule of aprotic solvents (carbon dioxide, two isotopomers of acetonitrile, and fluoroform) have been studied by rotational coherence spectroscopy (RCS) implemented with the time-resolved fluorescence depletion method. All of the observed RCS traces exhibit pronounced *C*-type transients, and this fact suggests that these species are quite close to planar asymmetric tops with their electronic transition moments pointing to in-plane directions. Weak *J*-type transients have been also identified for CNA−CO_2 and −CF_3H, the latter of which shows *A*-type transients as well. By comparing the experimental observations with density functional theory calculations at the B3LYP/6-31G(d,p) level, it is concluded that the solvent molecule is located by the side of the CN group of CNA with its molecular axis lying in the CNA molecular plane. All of the cluster geometries are of C_s symmetry, in which a positively charged atom of the solvents (C, H, or H for CO_2, CH_3CN, and CF_3H, respectively) is close to the cyano nitrogen of CNA, while an electonegative part (O, N, or F) contacts with the 1-position hydrogen of CNA. Some geometrical parameters including the centers of mass separation are obtained from the RCS-derived rotational constants.

1. Introduction

Reactivity and relaxation processes of aromatics are often influenced by solvents. Solvated clusters of aromatic molecules have been studied extensively to gain the microscopic description of these solvent effects. Among these studies, experimental characterization of cluster structure has a fundamental importance as follows. First, bonding nature, e.g., site, topology, and even strength, can be evaluated from geometrical information. Thus we can attain a detailed correlation between site-specific interaction and changes in electronic properties and dynamical behaviors of the chromophore. This is hardly achieved by studies in condensed media and is regarded as the most valuable aspect of studies on solvated aromatic clusters. Second, geometrical parameters are crucial inputs to specify intermolecular potential energy surfaces (IPSs). Many model IPSs have been constructed on the basis of quantum-mechanical calculations or empirical relations, mainly aiming to simulate solution structure. Comparison with experimentally derived data on cluster geometry will refine these models so as to reveal the solvent effects in condensed media on a molecular scale.

Because bonding character changes significantly for different solvents, systematic investigations with various solvent molecules are indispensable. To date, most extensively studied are clusters with protic solvents, e.g., water and alcohols. This is mainly due to recent development of double resonance spectroscopy implemented with IR or stimulated Raman excitation.[1−3] The method provides vibrational spectra associated with hydride stretching fundamentals, which are quite sensitive to site-specific hydrogen (H) bonding. Thus topologies of H-bonded clusters can be addressed quite well. Aromatics−(rare gas)$_n$ have been studied frequently also. Most of the studies have been conducted by microwave (MW)[4] or high-resolution laser[5] spectroscopy, which provide accurate spectroscopic data owing to their high frequency resolution. On the other hand, there have been limited numbers of reports on the structure of clusters with aprotic molecular solvents. This is probably because double resonance vibrational spectroscopy cannot afford definitive information on this class of clusters, because perturbation on vibrations is usually much smaller by weaker intermolecular interactions in the clusters. MW or high-resolution laser spectroscopy is also difficult (though not impossible) to apply because these clusters will accompany spectral congestion and weak intensity of individual lines due to inherently small rotational constants and possible interconversion motions.

Clusters of aromatic molecules with cyano group(s) have attracted considerable interest in the following aspects. The chromophores tend to act as electron acceptors due to large electronegativity of the CN group and often show intra- or intermolecular charge transfer (CT) reactions in solution. A typical example is 4-(*N*,*N*-dimethylamino)benzonitrile (DMABN). This molecule exhibits solvent dependent dual fluorescence, which has been attributed to the intramolecular CT-state formation in polar solvents.[6] So far, its clusters with various kinds of solvents have been studied to assess the CT reaction by microscopic solvation,[7−14] but it has been found that none of the 1:1 complexes of DMABN show CT fluorescence, even with polar solvents. From these observations, the solvent molecules are speculated to reside rather near the CN group than the aromatic ring, and it has been suggested that the interaction site of the solvent(s) to the chromophore is a controlling factor for the CT-state formation. Apparently, experimental characterization of their structures is crucial, which is not available at present.

* Corresponding author. FAX: +81-75-753-3974. e-mail: ohshima@kuchem.kyoto-u.ac.jp.

† Also Core Research for Evolutional Science and Technology (CREST), Japan Science and Technology Corporation (JST).

10.1021/jp0102771 CCC: $20.00 © 2001 American Chemical Society
Published on Web 04/19/2001

Site-dependent dynamics has been also examined for relaxation processes in an analogous molecule, benzonitrile. It has been shown that several 1:1 clusters have different decay rates of vibrationally excited states in the S_0 manifold, and this has been correlated to (probably) different bonding topologies of the solvents.[15] Among the clusters, the structure of benzonitrile−water has been established by rotational contour analysis,[16] MW,[17−20] high-resolution laser,[18] and double resonance vibrational spectroscopy:[15,21] it is planar in which water is H-bonded almost perpendicularly to the CN group. Benzonitrile−methanol has been shown to possess similar bonding topology.[21] In the cluster with argon, the rare gas atom lies on the aromatic plane, as confirmed by MW and high-resolution laser spectroscopy.[22,23] Structures of benzonitrile with acetonitrile, chloroform, and fluoroform have been considered from combinations of molecular orbital calculations, rotational contour analysis, and vibrational spectroscopy,[15] but it seems necessary to confirm by further investigation. Solvated clusters of cyanonaphthalene (CNN) have been also studied in some detail. It has been shown that solvation with polar molecules, e.g., diethyl ether, methanol, and acetonitrile, causes modification of the electronic and vibronic coupling in the chromophore, whereas nonpolar solvents provide essentially no effects.[24] Model calculations on solvent topologies and spectral shifts have been performed for clusters of CNN with acetonitrile and water molecules.[25]

In the present paper, we report the structural characterization of 1:1 clusters of 9-cyanoanthracene (CNA) with aprotic solvents, i.e., carbon dioxide, acetonitrile, and fluoroform, by applying rotational coherence spectroscopy (RCS).[26] Because RCS is a time-domain variant with rotational resolution, it provides structural information irrespective of the bonding character of the species to be studied, as can its frequency-domain counterparts, e.g., MW or high-resolution laser spectroscopy. In addition, RCS can be applied to species larger than can be studied by frequency-domain spectroscopy, though the derived data are not as accurate as MW or high-resolution laser spectroscopy. In this respect, this method is particularly suitable to our studies for systematic characterization of the solvation structure of CNA clusters.[27,28] For instance, we have already reported that CNA−water has a planar structure with the H-bonding water in the side of the CN group,[27] which is similar to the benzonitrile cluster. The present RCS results allow us to determine rotational constants of CNA−CO_2, −CH_3CN (and −CD_3CN), and −CF_3H. Density functional calculations at the B3LYP/6-31G(d,p) level have been performed to support the experimental observations. From these data, bonding topologies of the clusters are uniquely derived, and some of the structural parameters are extracted. On the basis of the present results, we make some consideration of the geometry of the solvated clusters containing cyano aromatics, which have been studied so far as mentioned above.

2. Experimental and Computational Procedures

2.1. RCS and LIF Measurements. Details on the present experimental setup have been described elsewhere.[28] The present RCS experiments were performed by utilizing time-resolved fluorescence depletion (TRFD)[29] with a solid-state picosecond laser system. It is composed of a femtosecond mode-locked Ti:sapphire laser (Spectra Physics, Tsunami) pumped by a diode-pumped cw Nd:YVO_4 laser (Spectra Physics, Millennia) and a picosecond regenerative amplifier (Spectra Physics, Spitfire) pumped by a Q-switched Nd:YLF laser (Spectra Physics, Merlin). The amplified output was 0.5 mJ per pulse at a repetition rate of 1 kHz, with the pulse width of ≈1 ps (fwhm) and the bandwidth below 1 nm. The fundamental of the ps laser light was frequency-doubled in an $LiBO_3$ crystal to produce excitation pulses for transitions of the species to be studied. The second harmonic thus obtained was directed through a Michelson interferometer to generate pump and variably delayed probe pulses of equal intensity. The pump and probe pulse trains, polarized parallel to one another, were recombined and sent collinearly into a vacuum chamber after collimated to ≈1 mm in diameter. The pulse trains intersected supersonic free jets perpendicularly at a distance of 5 mm from an expansion orifice. The averaged output of the UV light was ≈50 μJ/pulse, and its spectral bandwidth was ≈0.2 nm.

Clusters of CNA were formed in supersonic free-jet expansions. CNA was vaporized in a sample reservoir directly attached to a cw nozzle, both of which were heated to ≈150 °C by a sheath heater surrounding them. The carrier gas consisted primarily of helium with a small amount of carbon dioxide (Ekikai Tansan), acetonitrile (Nacalai Tesque, GR grade), acetonitrile-d_3 (Euriso-top, 99.8% isotopic purity), or fluoroform (Daikin Kogyo), which was mixed in at room temperature by means of a needle-valve arrangement. It was regulated to be 5 atm and led into the reservoir of CNA. The gas sample containing a trace amount of vaporized CNA was expanded continuously into a vacuum chamber through a small orifice (70 μm in diameter). The pressure in the chamber was maintained at 5×10^{-4} Torr during the experiment.

Time-integrated fluorescence was collected using two quartz lenses, filtered with a sharp-cut long-pass filter to eliminate scattered light from the excitation pulse, and detected with a photomultiplier tube held perpendicularly to the laser and molecular beams. The fluorescence signal was preamplified, filtered by a 1 kHz high-pass filter, and fed into a boxcar integrator, whose output was finally stored by a personal computer as a function of the delay between the pump and probe pulses to yield a TRFD trace. A typical completed scan corresponds to an average of some dozens of individual traces, each of which was obtained by averaging 300 laser shots at each delay position.

Before the RCS measurements, laser-induced fluorescence (LIF) spectra of the CNA clusters were observed using a dye laser (Lambda Physik, SCANmate 2E) pumped by a 10 Hz XeCl excimer laser (Lambda Physik, COMPex 102). The UV light (bandwidth < 0.5 cm^{-1}) crossed the molecular jet 5 mm downstream of the cw nozzle. Fluorescence was detected and averaged with the same apparatus as used in the TRFD experiments.

2.2. Molecular Orbital Calculations. Ab initio and density functional theory (DFT) molecular-orbital calculations were carried out for the CNA molecule and its clusters with carbon dioxide, acetonitrile, and fluoroform. For CNA−CO_2, minimum-energy structures were searched for at the RHF/6-31G level with several initial configurations for the solvent. Optimizations have been conducted without any symmetry constraint. Initial geometry of the solute in the cluster was set to the optimized one for bare CNA with C_{2v} symmetry. The stable structures thus identified were further optimized by DFT calculations using the Becke3LYP functional[30,31] with the 6-31G(d,p) basis set. For CNA−acetonitrile and −fluoroform, initial configurations were set by taking the most stable structure of CNA−CO_2 as a reference. Vibrational analyses were conducted for such optimized structures to ensure that they are true potential minima and to obtain zero-point vibrational energy (ZPVE) corrections. The total binding energies, $-\Delta E^B$ and $-\Delta E^N$, were calculated

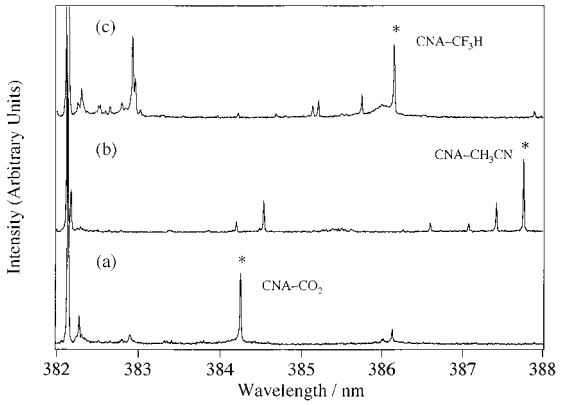

Figure 1. LIF spectra of the CNA clusters with (a) CO_2, (b) CH_3CN, and (c) CF_3H formed under jet-cooled conditions. Bands with asterisks are assigned to the S_1-S_0 origins of the corresponding 1:1 clusters, and monitored in RCS−TRFD measurements.

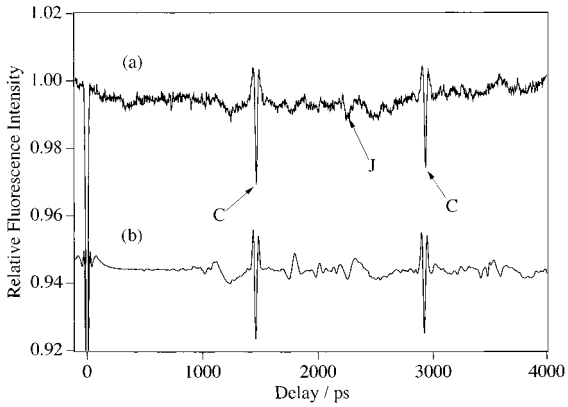

Figure 2. RCS traces of CNA−CO_2. (a) Experimental TRFD trace recorded with the band at $\delta\nu = -144$ cm^{-1}. Features labeled with C (J) are assigned to *C*-type (*J*-type) rotational coherence transients. (b) Simulated trace that reproduces the experimental one the best. Rotational constants are taken to the values listed in Table 3. The ratio of the *a*-, *b*-, and *c*- axis components of the transition dipole is 0.794:0.608:0.0. The horizontal scale indicates the relative intensity for the observed fluorescence, and the calculated trace is scaled to be similar to the experimental one.

with and without basis set superposition error (BSSE) corrections, respectively. The standard counterpoise procedure[32] was utilized to obtain the binding energies with BSSE corrections. All of the calculations were carried out with a suite of Gaussian 98 programs[33] on a personal computer.

3. Results

3.1. LIF Measurements. Figures 1a, b, and c show the LIF spectra of the CNA clusters with CO_2, CH_3CN, and CF_3H, respectively, in the region of 382−388 nm. The large peak at 382.13 nm (in air) in all of the spectra has been assigned to the origin of the S_1-S_0 electronic transition for the CNA monomer.[34] Adding a small amount of CO_2 to the CNA/He expansion produces several new bands as shown in Figure 1a. The band at 384.25 nm, with a shift ($\delta\nu$) of -144 cm^{-1} from the 0_0^0 band of bare CNA, is assigned to the electronic origin of the CNA−CO_2 cluster. Another much smaller band at $\delta\nu = -271$ cm^{-1} is probably due to the CNA−$(CO_2)_2$ cluster, judging from the intensity dependence on the CO_2 concentration. Because this band is not strong enough to perform RCS measurements, the present study is focused only on the 1:1 cluster. The CNA−CO_2 cluster does not show significant Franck−Condon activity in low-frequency intermolecular modes. Only a tiny peak at 382.90 nm will be assigned to a vibronic band associated with an intermolecular vibration of 92 cm^{-1}.

In Figure 1b, the red-most band at 387.76 nm ($\delta\nu = -380$ cm^{-1}) is assigned to the electronic origin of the 1:1 cluster of CNA with CH_3CN, because no other bands are observed to the red of this band. The band at 384.65 nm is located 216 cm^{-1} above the origin of the cluster, and thus assigned to a vibronic band with the 217 cm^{-1} intramolecular mode of CNA.[34] Furthermore, there appear two low-frequency progressions built on the origin and the 216 cm^{-1} bands of CNA−CH_3CN. Bands with up to two vibrational quanta are observed for a mode of 23 cm^{-1}. Bands with vibrational excess energy of 77 cm^{-1} are also observed. The LIF spectrum of CNA−CD_3CN is similar to Figure 1b, and the band origin is located at $\delta\nu = -381$ cm^{-1}. When increasing the concentration of acetonitrile in an attempt to observe 1:*n* clusters with $n \geq 2$, broad features develop around 385 and 390 nm but there appear no additional bands as sharp as those for the 1:1 cluster. This problem has also been found for solvated clusters of tetracene, fluorene,[35] and DMABN.[8]

For CNA−CF_3H, the band at $\delta\nu = -272$ cm^{-1} is assigned to the electronic origin of the 1:1 complex. A vibronic band 216 cm^{-1} above it is also observed at 382.96 nm. The band is partly overlapped with another stronger one at shorter-wavelength side (382.93 nm, $\delta\nu = -55$ cm^{-1}). Because these bands show similar intensity dependence on the solvent concentration, the band at $\delta\nu = -55$ cm^{-1} is provisionally attributed to an isomer of CNA−CF_3H. Unfortunately, the second isomer cannot be subjected to the RCS measurement because its origin band is so close ($\approx$2 cm^{-1}) to the 216 cm^{-1} band of the first isomer that they cannot be excited separately with our picosecond laser system. Several vibronic bands for intermolecular modes are also observed: some of them are 27, 63, and 68 cm^{-1} above the origin of the first isomer. The behavior of higher clusters between CNA and CF_3H is quite similar to the case with acetonitrile, where only broad features appear with higher solvent concentration.

3.2. RCS Measurements. To determine the rotational constants from the data, the RCS traces so obtained were compared with simulated ones. Simulations were carried out by using a program, coded in accord with the theoretical consideration by Felker and co-workers.[36−38] For simplicity, the ground-state expression for RCS transients was employed.[38] In performing the simulations the rotational temperature was assumed to be 5 K, for which the widths of observed transients were well reproduced. Because the laser pulse duration was much narrower than the TRFD transients, convolution was not necessary for simulating the RCS traces. In each of these simulations, the transition dipole, which is parallel to the in-plane short axis of the CNA moiety,[39] is assumed to be unchanged in the CNA fixed frame. Its principal-axis components are evaluated by considering the directional cosine matrix between the CNA-fixed and principal axes.

(*1*) *CNA−Carbon Dioxide*. Figure 2a shows an RCS−TRFD trace measured by monitoring the S_1-S_0 origin band of CNA−CO_2 at $\delta\nu = -144$ cm^{-1}. The raw trace showed an almost linearly changing baseline due to delay dependence in background fluorescence levels caused by lifetime effects,[29] delay-line misalignment, laser beam divergence, etc., and thus the trace shown in Figure 2a was subjected by baseline subtraction. The trace shows two prominent negative-going spikes (denoted with C's), representing a harmonic relation in their time delays with separation of $\approx$ 1466 ps. By comparing simulated traces calculated for probable cluster geometries as mentioned in section 4.1, they are assigned to *C*-type transients, which appear at $t \approx n/(4C)$ (*n* being an integer). A much weaker and broader

TABLE 1: RCS-Derived Rotational Constants of CNA Clusters (in GHz)[a]

	A	*B* + *C*	*C*
CNA−CO_2		0.431	0.171
CNA−CH_3CN			0.175
CNA−CD_3CN			0.169
CNA−CF_3H	0.486	0.311	0.133

[a] Estimated uncertainties are ±0.5%.

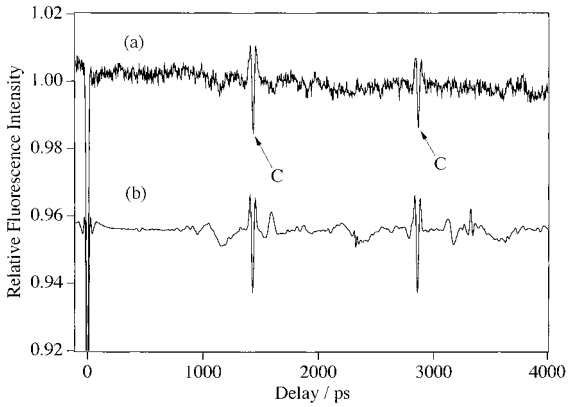

Figure 3. RCS traces of CNA-CH_3CN. (a) Experimental TRFD trace recorded with the band at $\delta\nu = -380$ cm^{-1}. Features labeled with C are assigned to *C*-type rotational coherence transients. (b) Simulated trace that reproduces the experimental one the best. Rotational constants are taken to the values listed in Table 3. The ratio of the *a*-, *b*-, and *c*-axis components of the transition dipole is 0.686:0.727:0.0.

transient with negative polarity at ≈2258 ps (denoted with J) is assigned to the second recurrence of *J*-type, which appears at $t \approx n/(2B + 2C)$ with $n = 2$. The corresponding recurrences with $n = 1$ and 3 cannot be identified because of the smaller intensities for odd *n*, in particular, in the case of low symmetry. The *C* and *B* + *C* rotational constants of CNA−CO_2 are determined from the positions of the RCS transients, as listed in Table 1. The widths of the transients are ≈20 ps (fwhm) or more, which set the uncertainties in the listed rotational constants (±0.5%).

(*2*) *CNA−Acetonitrile*. Figure 3a shows an RCS−TRFD trace measured for the S_1-S_0 origin band of CNA−CH_3CN at $\delta\nu = -380$ cm^{-1}, subjected by baseline subtraction. The trace is quite similar to that of CNA−CO_2, also exhibiting two prominent *C*-type transients. However, no *J*-type signals can be identified in this case. The *C*-type spacing (≈1433 ps) is only slightly smaller than that of CNA−CO_2. The similarity in the RCS traces implies a close resemblance in the cluster geometries for the both species, because the attached solvents possess comparable shapes and weights. The trace for CNA−CD_3CN exhibits analogous features, setting the *C*-type spacing to be 1478 ps. Accordingly, the *C* constants are determined for both CNA−CH_3CN and CNA−CD_3CN, as listed in Table 1.

(*3*) *CNA−Fluoroform*. Figure 4a shows an RCS−TRFD trace measured from the excitation of the 0_0^0 band of CNA−CF_3H at $\delta\nu = -272$ cm^{-1}, after baseline subtraction. Again, the trace is quite similar to that of CNA−CO_2, also exhibiting two prominent *C*-type transients spaced by ≈1883 ps. We can identify another two types of transients in the observed trace. One set, of which transients are spaced by ≈1590 ps with alternating polarity, is assigned to *J*-type on the basis of its characteristics. The trace also shows *A*-type transients, which appear at $t \approx n/(4A)$ (only *n* of multiples of three being apparent in this case) with positive polarity throughout the trace. Because the three different types of transients are observed, a complete set of the rotational constants is derived as listed in Table 1.

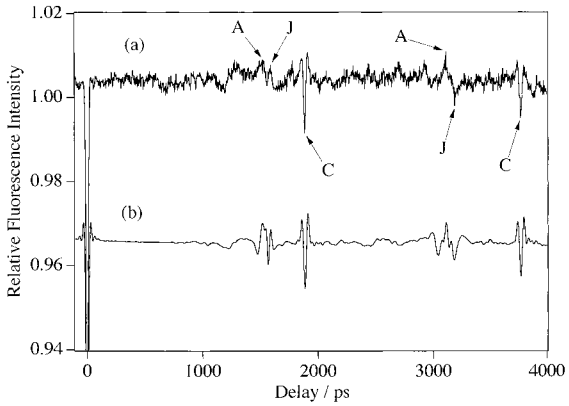

Figure 4. RCS traces of CNA−CF_3H. (a) Experimental TRFD trace recorded with the band at $\delta\nu = -272$ cm^{-1}. Features labeled with C, J, or A are assigned to *C*-, *J*-, or *A*-type rotational coherence transients. (b) Simulated trace that reproduces the experimental one the best. Rotational constants are taken from the values listed in Table 3. The ratio of the *a*-, *b*-, and *c*- axis components of the transition dipole is 0.834:0.552:0.0.

TABLE 2: DFT-Calculated Binding Energies, Geometrical Parameters, and Rotational Constants for CNA Clusters at the B3LYP/6-31G(d,p) Level

	CNA−CO_2 side-type	CNA−CO_2 T-type	CNA−CH_3CN	CNA−CF_3H
ΔE^N [a]/kcal mol^{-1}	−2.31	−1.94	−4.39	−4.52
ΔE^B [a]/kcal mol^{-1}	−1.13	−1.15	−3.07	−2.51
R[b]/Å	6.092	6.575	6.082	6.346
α[c]/deg	69.3	90	57.8	61.8
ϕ[d]/deg	130.5	0	133.3	190.4
r(N···X)[e]/Å	2.996	2.961	2.405	2.332
r(H_1···Y) [f]/Å	2.756		2.620	2.461
A/GHz	0.4856	0.4328	0.5485	0.4951
B/GHz	0.2556	0.2440	0.2509	0.1774
C/GHz	0.1675	0.1560	0.1724	0.1338

[a] Binding energy. The superscripts N and B represent without and with BSSE corrections, respectively. [b] Distance between the centers of mass of CNA and the solvent. [c] Angle between the *x* axis and the ***R*** vector. The axis system used is defined in the text. [d] Angle between the *x* axis and the molecular axis of the solvent. [e] Distance between the N atom of CNA and the nearest-neighbor atom X in the solvent (X = C, H, and H for CO_2, CH_3CN, and CF_3H, respectively). [f] Distance between the 1-position H atom of CNA and the nearest-neighbor atom Y in the solvent (Y = O, N, and F for CO_2, CH_3CN, and CF_3H, respectively).

3.3. Molecular Orbital Calculations. Two minimum-energy structures were obtained for CNA−carbon dioxide by geometry optimization at the DFT/B3LYP/6-31G(d,p) level. They are shown in Figures 5a and b, as side- and T-types, respectively. The carbon dioxide molecule lies in the CNA molecular plane in the both configurations. Calculated binding energies, geometrical parameters, and corresponding rotational constants are listed in Table 2. In the T-type isomer, the solvent is attached to the cyano group of the solute at the central carbon atom, with its molecular axis perpendicular to the C≡N axis. As a result, the structure is of C_{2v} symmetry. In the side-type isomer with C_s symmetry, CO_2 is shifted away approximately along the CNA long molecular axis from the position that it occupies in the T-type isomer. The molecular axis of CO_2 is tilted so that its oxygen atom seems to interact with the 1-position hydrogen atom of CNA. The binding energies of the two isomers are so close: those with BSSE corrections are essentially identical. Configurations with CO_2 on the CNA molecular plane have been identified as actually unbound. We, however, have to be aware that it does not necessarily exclude such types of structure as potential candidates, because the present level of

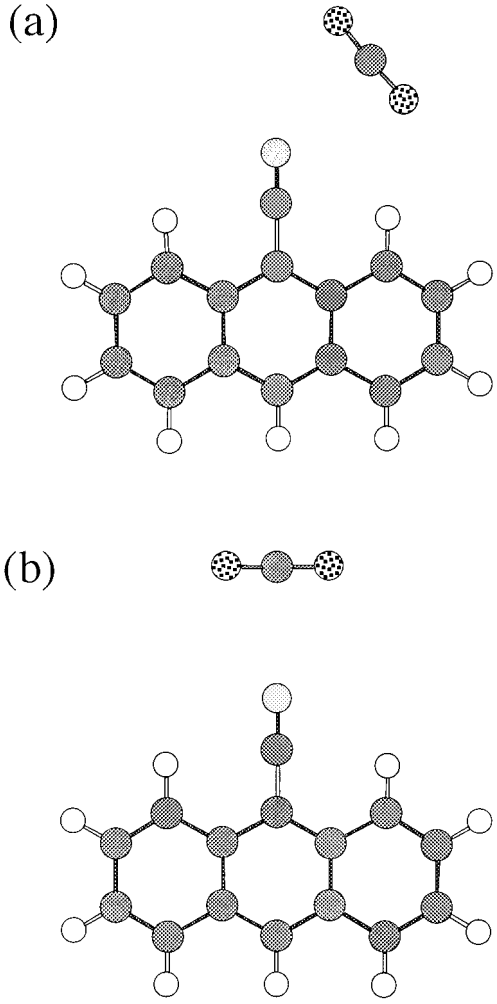

Figure 5. Two possible geometries of CNA−CO_2 predicted by the DFT/B3LYP/6-31G(d,p) calculations: (a) side-type and (b) T-type.

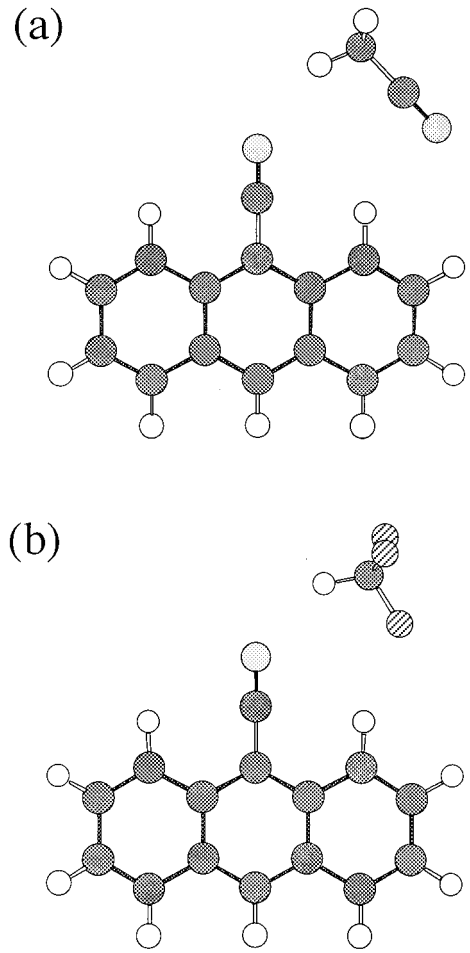

Figure 6. Geometries predicted by the DFT/B3LYP/6-31G(d,p) calculations for (a) CNA−CH_3CN and (b) CNA−CF_3H.

calculations should be far from sufficient to describe correctly the dispersion interaction between the π-electron clouds of solute and the solvents.[40]

For CNA−acetonitrile and CNA−fluoroform, DFT/B3LYP/6-31G(d,p) calculations identified minimum-energy structures similar to the side-type isomer of CNA−carbon dioxide. They are shown in Figures 6a and b, respectively. The C_3 symmetry axis of the solvent lies also in the CNA molecular plane. In CNA−acetonitrile, one of the methyl hydrogen atoms of the solvent points to the nitrogen atom in the CNA cyano group, making the structure as C_s symmetry. The cyano group of the solvent is in turn close to the 1-position of hydrogen atom of CNA. The solvent hydrogen atom in CNA−fluoroform also directs to the cyano nitrogen of the solute, while one of the fluorine atoms points to the 1-position hydrogen of CNA (C_s symmetry). Calculated binding energies, geometrical parameters, and corresponding rotational constants are listed in Table 2. Rotation around the C_3 axis by 60° gave an unstable configuration for both of the clusters. For CNA−fluoroform, a linear-type isomer, in which the solvent is collinearly H-bonded to the cyano nitrogen, was examined, but it has been found that such geometry corresponds to a transition state.

4. Analysis of Structures

In this section we use the RCS results reported above to ascertain effective zero-point geometrical parameters for the 1:1 CNA clusters with the aprotic solvents. In doing this, we make the usual assumption that the geometries of the chromophore[28] and solvents[41−43] do not change upon complexation. Note that in this work the observed rotational coherence effects represent the unresolved contributions of ground- and excited-state coherences.[37] Therefore, the structural parameters determined from the present RCS−TRFD data represent averages of the parameters in the two states.

The geometry of a molecular cluster is described by $6(n - 1) - l$ intermolecular degrees of freedom, n being the number of molecules that constitute the cluster and l being linear molecules among them.[44] Thus, there need to be five degrees of freedom to characterize the structure of CNA−carbon dioxide and six for CNA−acetonitrile and CNA−fluoroform. We here introduce an axis system, in which the origin is set to the CNA center of mass and the x and y axes direct along the long and short molecular axes of CNA, respectively, while z is perpendicular to the molecular plane. The (x, y, z) coordinates of a representative point (e.g., the center of mass) in the solvent are used to fix the solvent position relative to CNA. The orientation of the solvent with respect to the axis system is expressed with two polar coordinates (ϕ, θ) for carbon dioxide or three Eular angles (ϕ, θ, χ) for acetonitrile and fluoroform: (ϕ, θ) describe the angles made by the (C_∞ or C_3) symmetry axis of the solvent, and χ for rotation around the C_3 axis.

Because the x, y, and z axes are the principal axes of CNA, the moment-of-inertia tensor of the cluster represented in the axis system is related to the principal moments of inertia of the

constituents as[45]

$$I_{FF'}^{\text{cluster}} = \mu(R^2 - \delta_{FF'}R_F R_{F'}) + I_F^{\text{CNA}}\delta_{FF'} + \sum_g I_g^{\text{solvent}}\Phi_{Fg}\Phi_{F'g} \quad (1)$$

where F and $F' = x$, y, or z, and g is the index of the principal axes of the solvent molecule. The vector $\boldsymbol{R}$ with components R_F connects the centers of mass of CNA and the solvent, and μ is the reduced mass for them. Φ_{Fg} is the directional cosine matrix element, which is represented with the angles, ϕ, θ (and χ).[46]

When the molecular axis of the symmetric-top solvent lies in the CNA plane as in the T- and side-type structures, $R_z = 0$ and $\theta = 90°$. Then eq 1 is reduced as

$$I_a^{\text{cluster}} + I_b^{\text{cluster}} = \mu R^2 + I_x^{\text{CNA}} + I_y^{\text{CNA}} + I_\perp^{\text{solvent}} + I_{||}^{\text{solvent}} \quad (2)$$

$$(I_a^{\text{cluster}} - I_b^{\text{cluster}})^2 = [\mu R^2 \cos 2\alpha + I_y^{\text{CNA}} - I_x^{\text{CNA}} + (I_\perp^{\text{solvent}} - I_{||}^{\text{solvent}})\cos 2\phi]^2 + [\mu R^2 \sin 2\alpha + (I_\perp^{\text{solvent}} - I_{||}^{\text{solvent}})\sin 2\phi]^2 \quad (3)$$

$$I_c^{\text{cluster}} = \mu R^2 + I_z^{\text{CNA}} + I_\perp^{\text{solvent}} \quad (4)$$

where the angle α is made by the $\boldsymbol{R}$ vector and the x axis, and ϕ by the molecular axis of the solvent and the x axis. $I_{||}^{\text{solvent}}$ and $I_\perp^{\text{solvent}}$ are the principal moments of inertia of the solvent parallel and perpendicular to the molecular axis, respectively ($I_{||}^{\text{solvent}} = 0$ for a linear molecule). Thus, the distance R is directly evaluated from the C constant. It is noted that none of the principal moments (and accordingly the rotational constants) depend on χ when the solvent has an axial symmetry, and asymmetric isotopic substitution is necessary to fix the angle experimentally. Equations 2 and 4 lead to

$$I_a^{\text{cluster}} + I_b^{\text{cluster}} - I_c^{\text{cluster}} = I_{||}^{\text{solvent}} \quad (5)$$

This relation will serve to confirm that the solvent molecular axis lies in the CNA plane.

4.1. CNA−Carbon Dioxide. We first ascertain the gross geometry of CNA−CO_2 by comparing the experimental RCS trace with those simulated for the structures identified by the DFT calculations presented in section 3.3. Before doing this, we have checked the possibility that carbon dioxide resides on the aromatic plane of the CNA molecule in the observed cluster. It has been realized that the most prominent transients for those configurations should be of *J*-type, exhibiting the alternating polarity, with an appropriate distance between the molecules. In addition, the transients cannot be as strong as those denoted as "C" in the observed RCS trace (Figure 2a). Therefore, such conformations are ruled out as a possible structure of CNA−CO_2. The simulated traces for the side- and T-type structures predicted by the DFT calculations are shown in Figures 7a and b. Both of them exhibit strong *C*-type transients with negative polarity, which is qualitatively consistent with the observed trace. It is noted that the prominent transients of this type are common characteristics in the RCS traces for (nearly) planar asymmetric tops with the transition moment lying in the molecular plane.[47] This has been evidenced by previous studies on perylene,[48] carbazole−water and carbazole−ammonia,[49] 2,5-diphenyloxadiazole aggregates with one or two molecules of water and some alcohols,[50] 9,10-dichloroanthracene,[51] and bare CNA (ref 28) and CNA−water.[27] Quantitative match-up for the T-type is, however, far from acceptable: intervals between the *C*-type transients (≈1600 ps) are too large and the *J*-type transient at ≈2422 ps is too strong. On the other hand, the side-type isomer gives a satisfactory resemblance to the observed trace. From these facts, it is concluded that the gross geometry of CNA−CO_2 is of side-type.

TABLE 3: Geometrical Parameters Consistent with the Observed RCS Data and Corresponding Rotational Constants for CNA Clusters

	CNA−CO_2	CNA−CH_3CN[a]	CNA−CF_3H
R[b]/Å	5.94	5.92 (5.97)	6.37
α[c]/deg.	66.2	58.8 (59.9)	63.7
ϕ[d]/deg.	135	135	190
r(N···X)[e]/Å	3.04	2.27	2.37
r(H_1···Y) [f]/Å	2.65	2.56	2.51
A/GHz	0.500	0.537 (0.523)	0.486
B/GHz	0.260	0.259 (0.250)	0.178
C/GHz	0.171	0.175 (0.169)	0.133

[a] Values for CNA−CD_3CN are given in parentheses. [b] Distance between the centers of mass of CNA and the solvent. [c] Angle between the x axis and the $\boldsymbol{R}$ vector. The axis system used is defined in the text. [d] Angle between the x axis and the molecular axis of the solvent. [e] Distance between the N atom of CNA and the nearest-neighbor atom X in the solvent (X = C, H, and H for CO_2, CH_3CN, and CF_3H, respectively). [f] Distance between the 1-position H atom of CNA and the nearest-neighbor atom Y in the solvent (Y = O, N, and F for CO_2, CH_3CN, and CF_3H, respectively).

As the solvent lies in the CNA plane in the cluster, the distance R between the centers of mass is determined as listed in Table 3, by adopting eq 4 with the RCS-derived C constant of CNA−CO_2. The angles α and ϕ cannot be evaluated uniquely because there is only one additional experimental input, i.e., $B + C$ for a single isotopic species, but the derived value of α by adopting eq 3 is not sensitive to ϕ since the solvent moment of inertia is much smaller than those of the solute. Even when ϕ is varied in the entire region (0 to 180°), α falls within a relatively narrow range of ≈66.1−70.4°. Accordingly, the center of mass position of CO_2 change only by ±0.21 and ±0.08 Å along the x and y axes, respectively. The acceptable range is further reduced when the cluster geometry is constrained to be physically probable in respect of van der Waals (vdW) contact. If ϕ is out of the range from (130−140)° [the corresponding α = (66.3−66.1)°], the nearest distance between atoms in CO_2 and CNA becomes significantly (i.e., by > 0.2 Å) shorter than the sum of their vdW radii (C: 1.70 Å, N: 1.55 Å, O: 1.52 Å, H: 1.20 Å).[52] For a reference, geometrical parameters and the corresponding rotational constants for the structure with ϕ = 135° are listed in Table 3. The simulated RCS trace in Figure 2b, which is calculated on the basis of the structure, reproduces well the features appearing in the experimental one, including broad transients which do not correspond to any of *J*-, *K*-, *A*-, or *C*-type recurrence. This confirms the validity of the structure for CNA−CO_2 from the present analysis.

4.2. CNA−Acetonitrile. The geometrical structure of CNA−acetonitrile is expected to resemble that of CNA−CO_2 from the similarity between their RCS traces. This expectation is confirmed by the good match-up between the observed RCS trace (Figure 3a) and that simulated for the side-type structure predicted in section 3.3, as shown in Figure 7c. Then, we evaluate some geometrical parameters from the experimentally derived C rotational constants for CNA−CH_3CN and CNA−CD_3CN. The distances R between the centers of mass are determined for the two isotopic species as listed in Table 3. From these values we can fix the relative orientation of the $\boldsymbol{R}$ vector and the solvent molecular axis, but there is no information on the absolute value of α or ϕ due to the lack of experimentally

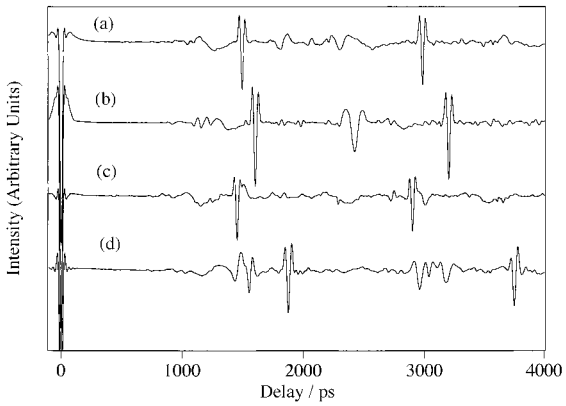

Figure 7. Simulated RCS traces corresponding to the four CNA clusters depicted in Figures 5 and 6: (a) side-type CNA−CO_2, (b) T-type CNA−CO_2, (c) CNA−CH_3CN, and (d) CNA−CF_3H.

derived *A* or *B* constants. Therefore, the angle ϕ is assumed to be the same (135°) for CNA−CO_2. This value is quite close to that from the DFT calculations, as listed in Table 2. We take here the *x* and *y* coordinates of the methyl C atom of acetonitrile as the variable parameters. The angle χ is fixed so that one of the methyl hydrogen (or deuterium) atoms in acetonitrile lies in the CNA molecular plane and points toward the cyano group. With these assumptions, values for several geometrical parameters are derived as listed in Table 3. The rotational constants for the geometry are also listed in the table. The RCS trace is simulated on the basis of the structure, as shown in Figure 3b. It reproduces the experimental trace reasonably well.

4.3. CNA−Fluoroform. The geometrical structure of the cluster is expected as the side-type predicted in section 3.3, because the simulated RCS trace for the structure, as shown in Figure 7d, resembles well the observed trace (Figure 4a). In this case, all three rotational constants have been obtained, and we can check whether or not eq 5 holds for the cluster. From the RCS-derived data, $I_a + I_b - I_c = 79$ uÅ^2 for CNA−CF_3H, which agrees with $I_{||} = 89$ uÅ^2 for bare CF_3H (ref 43) within the experimental uncertainty. Therefore, it is confirmed that the solvent C_3 symmetry axis is in the CNA plane. Then we evaluate geometrical parameters from the experimentally derived rotational constants. The distance *R* is evaluated as listed in Table 3 from the *C* constant. The angle α is found to be in the range of ≈62.1−66.2°, with ϕ varying from 0 to 360°. Unfortunately, the constraint for vdW contacts cannot be adopted in this case because shorter distances are predicted by the DFT calculations for the closest pairs of atoms in CNA and the solvent (see Table 2), probably due to stronger electrostatic interactions. In Table 3, some geometrical parameters and the corresponding rotational constants are listed when the angle ϕ is arbitrarily set to the value (190°) from the DFT calculations. The angle χ is fixed so that one of the fluorine atoms lies in the CNA molecular plane and points toward the 1-position hydrogen of CNA. The RCS trace is simulated on the basis of the structure, as shown in Figure 4b. Its match-up with the experimental trace is satisfactory.

5. Discussion

From the RCS-derived data combined with the DFT calculations, gross geometries of the observed 1:1 CNA clusters with the aprotic solvents (CO_2, acetonitrile, and CF_3H) have been identified as side-type, which are represented pictorially in Figures 5a, 6a, and 6b, respectively. The previous study on CNA−water has shown that the solvent is also bound sidewise to the CN group of CNA.[27] Thus, the bonding topologies in the solvated clusters of CNA are quite similar to each other, even though the attaching molecules are usually classified into different categories: water as protic, CO_2 as nonpolar aprotic, and acetonitrile and CF_3H as polar aprotic solvents. The obtained geometries imply that, among the intermolecular attractive forces, the electrostatic interaction characterizes predominately the solvation structures in the clusters. Positively and negatively charged parts of the solvents contact respectively with the electronegative cyano group and the 1-position hydrogen with partially positive charge in the solute. The similarity in solvation topologies can be rationalized by the large nonuniformity of charge distributions in the solvent molecules: water, acetonitrile, and CF_3H have large polarity as evidenced by their electric dipole moments (1.854, 3.924, and 1.651 D, respectively),[53] whereas nonpolar CO_2 actually possesses substantially polarized bonds, as verified by its electric quadrupole moment (-4.3×10^{-26} esu).[54]

The DFT-predicted rotational constants listed in Table 2 are in good agreement with those determined experimentally listed in Table 1. The calculated values are smaller only by ≈2% for CNA−CO_2 and −CH_3CN, and the differences are even smaller for CNA−CF_3H. This fact validates the structural parameters listed in Table 3, which have been derived with some assumptions based on the DFT results. Characteristics of the solvation structures of the clusters, including CNA−water,[27] are summarized as follows. First, both the interactions at two different sites are essential to maximize the total stability, though the orientation of the solvents deviates from the optimum for each of the sites due to the competition between the interactions. Such competing nature of site-specific interactions will be discussed in relation with possible multiple conformations in the following. Second, interactions between the CNA cyano group and the positively charged atom (here denoted as X) in the solvents (X = H for H_2O, CH_3CN, and CF_3H, and C for CO_2) seem to be rather strong, judging from the distances between the cyano N atom and X (see Table 3). For the pair in CNA−CO_2, the distance is shorter by ≈0.2 Å than the sum of the vdW radii. The differences are ≈0.4−0.5 Å for the clusters with CH_3CN and CF_3H, though the assumption on ϕ may provide some uncertainties. These shortenings from the vdW contacts are not so different from that in CNA−water (≈0.6 Å).[27] The CN···H−C bonding can thus be regarded as an H-bond, and CH_3CN and CF_3H act as proton donors to a bonding site with high electronegativity (e.g., cyano group). Third, interactions involving the 1-position hydrogen of CNA are also important, as indicated by the distances to the nearest-neighbor atom (here denoted as Y) with substantial electronegativity in the solvents (Y = O for H_2O and CO_2, N for CH_3CN, and F for CF_3H). The shortenings from the vdW contacts are ≈0.1−0.2 Å in this case. Recently, such H-bonds concerning aromatic C−H bonds have been identified in several clusters with an aromatic chromophore with protic solvents.[3,17−21,27,55,56] The present results afford an experimental evidence of such bonding pertained by the aprotic solvents.

For CNA−CO_2 and CNA−acetonitrile, only one species is observed in supersonic expansions, in which the internal temperatures are very low (on the order of 10 K). Therefore, it is highly probable that they are the most stable forms as the 1:1 clusters, which are identified as the side-type by the present RCS study. In the case of CNA−CO_2, the DFT calculations at the B3LYP/6-31G(d,p) level have predicted the T-shaped form as stable as the side-type. However, the vibrational analysis on this conformation gives an extremely low frequency mode (3.7 cm^{-1}) that corresponds to a translational motion of the solvent

approximately along the *x* direction. Thus, it might be a transition state collapsing into the side-type, when higher level calculations are applied. It is noted that the T-shaped form is the conformation that maximizes the electrostatic interaction between the quadrupole moment of CO_2 and the dipole moment of the CN group.[44] Whether or not the T-shaped conformation is a true minimum, it is definitely less stable than the side-type. This shows the importance of the H-bonding at the 1-position H atom in CNA, which compensates the destabilization in the electrostatic interaction at the CN site. Another possible conformation for the cluster is a π-type, in which the solvent lies on the CNA aromatic plane due predominately to the dispersion interaction with the π-electrons of the solute. This conformation is a common structural motif for rare-gas clusters, such as CNA$-(Ar)_n$ ($n = 1-3$).[28] The binding energy for CNA$-$Ar is estimated as $\approx$1.3$-$1.4 kcal/mol, by adopting simple pairwise atom$-$atom additive potentials.[28,57,58] This is almost the same as the DFT-predicted binding energy for CNA$-CO_2$ (see Table 2). Because the average polarizability of CO_2 (2.91 Å^3) is much larger than Ar (1.64 Å^3),[53] the π-type bonding in CNA$-CO_2$ must be stronger than CNA$-$Ar. More elaborated study is necessary to give a definitive conclusion on the existence of π-type isomer(s), though the DFT/B3LYP/6-31G(d,p) calculations have obtained no stable conformation of this type.

For CNA$-CF_3H$, an additional species has been observed with comparable intensity in addition to the side-type isomer identified by RCS. It must be another conformational isomer, of which the definitive characterization must await for further study. The side-type isomer shows a much larger spectral red shift ($\delta\nu = -272$ cm^{-1}) in the S_1-S_0 transition than does the other one ($\delta\nu = -55$ cm^{-1}). Site-dependent perturbation on electronic excitation will be discussed in detail once the structure of the other isomer is established. One of the possible conformations is a π-type, because the average polarizability of CF_3H (3.57 Å^3)[53] is also substantially larger than Ar. The linear-type form has been predicted as a transition state by the DFT/B3LYP/6-31G(d,p) calculations, as mentioned in section 3.3, so it is unlikely that the species is of this type. It is noted that linear-type conformation gives the maximum stability to the electrostatic interaction between two dipole moments,[44] and the importance of the H-bonding at the 1-position H atom in CNA is verified also in this case, because one of the most stable forms is the side-type.

Geometries of several 1:1 clusters containing a related cyano aromatic chromophore have been discussed,[10,12,15-25] as mentioned briefly in the Introduction. Some protic as well as aprotic solvents, including acetonitrile and CF_3H, have been examined in these studies. The structure of benzonitrile$-CH_3CN$ has been considered as a side-type, on the basis of vibrational spectra measured by double resonance spectroscopy and Hartree$-$Fock (HF) level calculations with the 6-31G(d,p) basis set.[15] Model potential calculations have identified that the most stable geometries for the 1- and 2-CNN clusters are the same types.[25] There are two side-type isomers in this case, because sidewise bonding to the CN group provides two nonequivalent sites. Consequently, the side-type conformation is confirmed as the common bonding topology in the most stable forms of the cyano aromatics solvated with an acetonitrile molecule. This type of geometry must be also important in DMABN$-CH_3CN$, though the previous study did not consider it.[10] Benzonitrile$-CF_3H$ has been considered as a linear-type from vibrational spectra and HF/6-31G(d,p) calculations.[15] This is in contrast with the present results on the CNA cluster, which is established as the side-type. Of course bonding topologies are determined by subtle balance of intermolecular interactions and may differ for two closely related clusters. Nevertheless, the results on the benzonitrile cluster are likely to be considered more carefully. First, it seems that probable stable geometries have not be explored intensively. For instance, the same level of calculation has shown that both the linear- and side-types are local minima for CNA$-CF_3H$. Second, higher-level calculations are necessary for a definitive conclusion, as evidenced by the fact that the linear-type CNA$-CF_3H$ becomes a transition state by the B3LYP-DFT calculations with the same basis set. Third, comparison of the observed and calculated vibrational spectra may not provide decisive information on the cluster geometry in this case, because the shifts are quite small and some of the observed bands are perturbed by anharmonic resonance. Experimental proof will be given by studies with rotational resolution either in frequency or time domain. As a summary of the structural motif of microsolvation, a solvent molecule lies in the aromatic plane and contacts with the CN group of an aromatic chromophore, if it has substantially nonuniform charge distribution (either protic or aprotic). This is generally in accord with the speculation that polar solvents in the DMABN clusters perturb the aromatic ring of the chromophore to much less extent.[7-10]

Finally, we discuss possible interconversion motions in the clusters. The internal rotation around the symmetry axis of acetonitrile may be feasible to give a measurable tunneling splitting, even in the vibrational ground state. Such a motion splits each rovibronic level into two with *A* and *E* symmetries with respect to the C_3 rotational group.[59] The two levels couple respectively with different nuclear spin states associated with three equivalent H (or D) atoms, so that both of them are populated in proportion to the corresponding statistical weights, even in adiabatically cooled conditions. If rotational constants are substantially different for the *A* and *E* states, RCS transients will be observed as doublet. This is not the case in the present observation. There are two possible explanations for the absence of the tunneling splitting. First, it is expected that the barrier for the internal rotation is too high to give an observable splitting. It may be reasonable because one of the methyl H (or D) atom is H-bonded to the CN group. Second, the internal-rotation angular momentum directs along the symmetry axis and has no *c*-axis component (perpendicular to the CNA molecular plane). Accordingly, the rotational term values that are related exclusively to the *C* constants will be preserved even by excitation of the internal rotation so as to give *C*-type transients for the *A* and *E* states at the same positions. Other types of transients (e.g., *J*- and *A*-types) may be affected, but they are too small to be detected. Rigorous treatments of internal rotation in RCS have not been considered so far and will be an interesting subject. In the case of CNA$-CF_3H$, the internal-rotation tunneling must be negligible, because it has not been observed in the related, more floppy systems Ar$-PF_3$ and Kr$-PF_3$.[60]

6. Conclusion

We have presented the structural characterization of the 1:1 CNA clusters with aprotic solvents, i.e., carbon dioxide, acetonitrile, and fluoroform, on the basis of the experimental attainments by rotational coherence spectroscopy. The gross structures of the species have been determined as side-type, as is the case of the CNA$-$water cluster, in which the solvent molecule interacts with the CNA chromophore at two sites, the nitrogen atom of the cyano group and the 1-position hydrogen atom. The present results support most parts of the previous

structural implication of related solvated clusters containing cyano aromatics such as benzonitrile[15] and cyanonaphthalene[25] addressed by calculations or double resonance vibrational spectroscopy, though the proposed structure for benzonitrile−fluoroform differs qualitatively from the determined one for the CNA cluster. Rotational constants obtained from the RCS results have allowed us to extract some of the structural parameters, under the assumption that the solvent symmetry axis lies in the molecular plane of CNA. It has been shown that DFT predicted values agree quite well with the experimentally determined values.

Acknowledgment. The present work has been supported by Grants-in-Aid (Nos. 08454177 and 10440172) from the Ministry of Education, Science, Culture, and Sports of Japan. Additional support has been provided from Japan Science and Technology Corporation (JST). Y.O. thanks the Mitsubishi Chemical Foundation, the Japan Securities Scholarship Foundation, and Asahi Glass Foundation for financial support.

References and Notes

(1) Felker, P. M.; Maxton, P. M.; Schaeffer, M. W. *Chem. Rev.* **1994**, *94*, 1787.
(2) Zwier, T. S. *Annu. Rev. Phys. Chem.* **1996**, *47*, 205.
(3) Brutschy, B. *Chem. Rev.* **2000**, *100*, 3891.
(4) Bettens, F. L.; Bettens, R. P. A.; Bauder, A. In *Jet Spectroscopy and Molecular Dynamics*; Hollas, J. M., Phillips, D., Eds.; Chapman and Hall: London, 1995; Chapter 1.
(5) Neusser, H. J.; Sussmann, R. In *Jet Spectroscopy and Molecular Dynamics*; Hollas, J. M., Phillips, D., Eds.; Chapman and Hall: London, 1995; Chapter 4.
(6) Lippert, E.; Rettig, W.; Bonacic-Koutecky, V.; Heisel, F.; Miehe, J. A. *Adv. Chem. Phys.* **1987**, *68*, 1.
(7) Kobayashi, T.; Futakami, M.; Kajimoto, O. *Chem. Phys. Lett.* **1986**, *130*, 63.
(8) Gibson, E. M.; Jones, A. C.; Phillips, D. *Chem. Phys. Lett.* **1987**, *136*, 454.
(9) Peng, L. W.; Dantus, M.; Zewail, A. H.; Kemnitz, K.; Hicks, J. M.; Eisenthal, K. B. *J. Phys. Chem.* **1987**, *91*, 6162.
(10) Warren, J. A.; Bernstein, E. R.; Seeman, J. I. *J. Chem. Phys.* **1988**, *88*, 871.
(11) Grassian, V. H.; Warren, J. A.; Bernstein, E. R.; Secor, H. V. *J. Chem. Phys.* **1989**, *90*, 3994.
(12) Kajimoto, O.; Yokoyama, H.; Ooshima, Y.; Endo, Y. *Chem. Phys. Lett.* **1991**, *179*, 455.
(13) Shang, Q.-Y.; Bernstein, E. R. *J. Chem. Phys.* **1992**, *97*, 60.
(14) Howell, R.; Phillips, D.; Petek, H.; Yoshihara, K. *Chem. Phys.* **1994**, *188*, 303.
(15) Yamamoto, R.; Ishikawa, S.; Ebata, T.; Mikami, N. *J. Raman Spectrosc.* **2000**, *31*, 295.
(16) Kobayashi, T.; Honma, K.; Kajimoto, O.; Tsuchiya, S. *J. Chem. Phys.* **1987**, *86*, 1111.
(17) Storm, V.; Consalvo, D.; Dreizler, H. *Z. Naturforsch.* **1997**, *52a*, 293.
(18) Helm, R. M.; Vogel, H.-P.; Neusser, H. J.; Storm, V.; Consalvo, D.; Dreizler, H. *Z. Naturforsch.* **1997**, *52a*, 655.
(19) Storm, V.; Dreizler, H.; Consalvo, D. *Chem. Phys.* **1998**, *239*, 109.
(20) Melandri, S.; Consalvo, D.; Caminati, W.; Favero, P. G. *J. Chem. Phys.* **1999**, *111*, 3874.
(21) Ishikawa, S.; Ebata, T.; Mikami, N. *J. Chem. Phys.* **1999**, *110*, 9504.
(22) Dahmen, U.; Stahl, W.; Dreizler, H. *Ber. Bunsen-Ges. Phys. Chem.* **1994**, *98*, 970.
(23) Helm, R. M.; Vogel, H.-P.; Neusser, H. J. *Chem. Phys. Lett.* **1997**, *270*, 285.
(24) Lahmani, F.; Zehnacker-Rentien, A.; Breheret, E. *J. Chem. Phys.* **1990**, *94*, 8767.
(25) Brenner, V.; Zehnacker, A.; Lahmani, F.; Millié, E. *J. Chem. Phys.* **1993**, *97*, 10570.
(26) Felker, P. M. *J. Phys. Chem.* **1992**, *96*, 7844.
(27) Egashira, K.; Ohshima, Y.; Kajimoto, O. *Chem. Phys. Lett.* **2001**, *334*, 285.
(28) Egashira, K.; Ohshima, Y.; Kajimoto, O. *J. Phys. Chem. A*, **2001**, *105*, 1131.
(29) (a) Côté, M. J.; Kauffman, J. F.; Smith, P. G.; McDonald, J. D. *J. Chem. Phys.* **1989**, *90*, 2865. (b) Kauffman, J. F.; Côté, M. J.; Smith, P. G.; McDonald, J. D. *ibid.* **1989**, *90*, 2874.
(30) Lee, C.; Yang, W.; Parr, R. G. *Phys. Rev. B* **1988**, *37*, 785.
(31) Becke, A. D. *J. Chem. Phys.* **1993**, 98, 5648.
(32) Boys, S. F.; Bernardi, F. *Mol. Phys.* **1970**, *19*, 553.
(33) Frisch, M. J.; Trucks, G. W.; Schlegel, H. B.; Scuseria, G. E.; Robb, M. A.; Cheeseman, J. R.; Zakrzewski, V. G.; Montgomery, J. A., Jr.; Stratmann, R. E.; Burant, J. C.; Dapprich, S.; Millam, J. M.; Daniels, A. D.; Kudin, K. N.; Strain, M. C.; Farkas, O.; Tomasi, J.; Barone, V.; Cossi, M.; Cammi, R.; Mennucci, B.; Pomelli, C.; Adamo, C.; Clifford, S.; Ochterski, J.; Petersson, G. A.; Ayala, P. Y.; Cui, Q.; Morokuma, K.; Malick, D. K.; Rabuck, A. D.; Raghavachari, K.; Foresman, J. B.; Cioslowski, J.; Ortiz, J. V.; Stefanov, B. B.; Liu, G.; Liashenko, A.; Piskorz, P.; Komaromi, I.; Gomperts, R.; Martin, R. L.; Fox, D. J.; Keith, T.; Al-Laham, M. A.; Peng, C. Y.; Nanayakkara, A.; Gonzalez, C.; Challacombe, M.; Gill, P. M. W.; Johnson, B.; Chen, W.; Wong, M. W.; Andres, J. L.; Gonzalez, C.; Head-Gordon, M.; Replogle, E. S.; Pople, J. A. *Gaussian 98*; Gaussian, Inc.: Pittsburgh, PA, 1998.
(34) Amirav, A.; Horwitz, C.; Jortner, J. *J. Chem. Phys.* **1988**, *88*, 3092.
(35) Even, U.; Jortner, J. *J. Chem. Phys.* **1983**, *78*, 3445.
(36) Felker, P. M.; Zewail, A. H. *J. Chem. Phys.* **1987**, *86*, 2460.
(37) Hartland, G. V.; Connell, L. L.; Felker, P. M. *J. Chem. Phys.* **1991**, *94*, 7649.
(38) Felker, P. M.; Zewail, A. H. In *Femtosecond Chemistry*; Manz, J.; Wöste, L., Ed.; VCH: Weinheim, 1995; Vol. I, Chapter 5.
(39) Macfarlane, R. M.; Philpott, M. R. *Chem. Phys. Lett.* **1976**, *41*, 33.
(40) Kristyán, S.; Pulay, P. *Chem. Phys. Lett.* **1994**, *229*, 175.
(41) Courtoy, C. P. *Can. J. Phys.* **1957**, *35*, 608.
(42) Costain, C. C. *J. Chem. Phys.* **1958**, *29*, 864.
(43) Ghosh, S. N.; Trambarulo, R.; Gordy, W. *J. Chem. Phys.* **1952**, *20*, 605.
(44) Stone, A. J. *The Theory of Intermolecular Forces*; Oxford University Press: Oxford, 1996.
(45) Connell, L. L.; Ohline, S. M.; Joireman, P. W.; Corcoran, T. C.; Felker, P. M. *J. Chem. Phys.* **1992**, *96*, 2585.
(46) Zare, R. N. *Angular Momentum. Understanding Spatial Aspects in Chemistry and Physics*; John Wiley: New York, 1988; p 81.
(47) Joireman, P. W.; Connell, L. L.; Ohline, S. M.; Felker, P. M. *J. Chem. Phys.* **1992**, *96*, 4118.
(48) Ohline, S. M.; Joireman, P. W.; Connell, L. L.; Felker, P. M. *Chem. Phys. Lett.* **1992**, *191*, 362.
(49) Joireman, P. W.; Ohline, S. M.; Connell, L. L.; Felker, P. M. *J. Phys. Chem.* **1993**, *97*, 12504.
(50) (a) Troxler, T.; Smith, P. G.; Topp, M. R. *Chem. Phys. Lett.* **1993**, *211*, 371. (b) Troxler, T.; Smith, P. G.; Stratton, J. R.; Topp, M. R. *J. Chem. Phys.* **1994**, *100*, 797.
(51) Ohline, S. M.; Romascan, J.; Felker, P. M. *J. Phys. Chem.* **1995**, *99*, 7311.
(52) Bondi, A. *J. Phys. Chem.* **1964**, *68*, 441.
(53) Lide, D. R., Ed., *CRC Handbook of Chemistry and Physics*; CRC: Boca Raton, 1997.
(54) Buckingham, A. D.; Disch, R. L.; Dunmur, D. A. *J. Am. Chem. Soc.* **1968**, *90*, 3104.
(55) Mitsui, M.; Ohshima, Y.; Ishiuchi, S.; Sakai, M.; Fujii, M. *Chem. Phys. Lett.* **2000**, *317*, 211.
(56) (a) Mitsui, M.; Ohshima, Y. *J. Phys. Chem. A* **2000**, *104*, 8638. (b) Mitsui, M.; Ohshima, Y., Ishiuchi, S.; Sakai, M.; Fujii, M. *ibid.* **2000**, *104*, 8649.
(57) Troxler, T.; Leutwyler, S. *J. Chem. Phys.* **1993**, *99*, 4363.
(58) Uridat, D.; Brenner, V.; Dimicoli, I.; Le Calvé, J.; Millié, P.; Mons, M.; Piuzzi, F. *Chem. Phys.* **1998**, *239*, 151.
(59) Ford, R. S.; Suenram, R. D.; Fraser, G. T.; Lovas, F. J.; Leopold, K. R. *J. Chem. Phys.* **1991**, *94*, 5306.
(60) Taleb-Bendiab, A.; LaBarge, M. S.; Lohr, L. L.; Taylor, R. C.; Hillig, K. W., II; Kuczkowski, R. L.; Bohn, R. K. *J. Chem. Phys.* **1989**, *90*, 6949.